

Electron microscopy (HREM, EELS) study of the reoxidation conditions for recovery of NM/CeO₂ (NM: Rh, Pt) catalysts from decoration or alloying phenomena

S. Bernal, G. Blanco, J.J. Calvino*, C. López-Cartes, J.A. Pérez-Omil, J.M. Gatica, O. Stephan^a and C. Colliex^a

Departamento de Ciencia de los Materiales, Ingeniería Metalúrgica y Química Inorgánica, Facultad de Ciencias, Universidad de Cádiz, C/República Saharaui s/n, Apartado 40, Puerto Real, 11510 Cádiz, Spain

E-mail: jose.calvino@uca.es

^aLaboratoire de Physique des Solides, CNRS URA 002, Université Paris-Sud, Bâtiment 510, 91405 Orsay Cedex, France

Received 3 April 2001; accepted 10 July 2001

The reversibility of metal–support interaction effects in NM/CeO₂ catalysts (NM: Rh, Pt) is investigated using high-resolution electron microscopy and electron energy loss spectroscopy. Reoxidation treatments at 773 K followed by a mild reduction at 473 K are not effective in recovering ceria-based systems from the decorated or alloyed states observed upon high-temperature reduction ($T_{\text{red}} > 973$ K).

KEY WORDS: NM/CeO₂ catalysts; recovery from strong metal–support interaction; reoxidation temperature; HREM and EELS studies

1. Introduction

Since the pioneering works by Naccache and coworkers [1,2] on Pt/CeO₂, many authors have reported significant perturbations of the chemisorptive [3,4] and catalytic [5–7] properties of NM/CeO₂ catalysts (NM: Rh, Pt) on increasing the reduction temperature. Most of these studies have dealt with catalysts reduced at temperatures not higher than 773 K, a reference reduction treatment which is well known to induce the so-called SMSI (strong metal–support interaction) state in titania-supported metal catalysts [8–10].

Several authors have interpreted the deactivation phenomena occurring on NM/CeO₂ catalysts reduced at 773 K or even lower temperatures in terms of the occurrence of a SMSI-like effect. Though not proved sufficiently, Pt–Ce alloying [1,2] and metal decoration phenomena [11–13] have been proposed as a likely origin of the observed effects.

In spite of these proposals, there are numerous experimental data suggesting some significant differences between ceria- and titania-supported catalysts. Thus, on ceria-based catalysts reduced at 773 K, partial rather than strong inhibition of their hydrogen chemisorptive properties is usually observed. This seems to be the case for both Pt/CeO₂ [14,15] and Rh/CeO₂ [3,16–18], samples. On Rh/CeO₂, no suppression of the metal chemisorption capability could even be observed upon reduction at 1000 K [19]. Similar observations have recently been reported for the chemisorptive behaviour of Rh/Ce_{0.68}Zr_{0.32}O₂ [20] and Pt/Ce_{0.68}Zr_{0.32}O₂ [21]. Moreover, the comparison of the behaviours exhibited by the two catalysts above [20,21] strongly suggests that platinum is more sensitive than rhodium to the chemical deactivation

effects induced by the progressive increase of the reduction temperature.

High-resolution electron microscopy (HREM) studies have also provided clues about the difference existing between the nature of metal–support interaction effects in ceria- and titania-supported metal catalysts. Nowadays, a good deal of information is available about the nanostructural evolution undergone by both Pt/CeO₂ [15,22–25] and Rh/CeO₂ [16,26–29] catalysts upon increasing the reduction temperature. Reduction treatments ranging from 473 up to 1173 K have been investigated. All the HREM studies above [15,16,22–29] have agreed on the absence of metal decoration or alloying phenomena on catalysts reduced at 773 K or lower temperatures. Also worth of noting is that, for $T_{\text{red}} \leq 773$ K, the reduction temperature has a minor effect on the metal particle size distribution, and therefore, on the metal dispersion [26].

By contrast, on catalysts reduced at 973 K, the HREM images have clearly shown the occurrence of metal decoration effects on both Rh/CeO₂ [27] and Pt/CeO₂ [23]. Likewise, the combined application of experimental HREM and computer simulation techniques have only proved the occurrence of Pt–Ce alloying phenomena at the highest reduction temperature: 1173 K [23]. To summarise, in NM/CeO₂ (NM: Rh, Pt) catalysts, the onset of the nanostructural phenomena associated with the SMSI effect requires reduction temperatures well above 773 K. The same is true for a number of ceria-based mixed-oxide-supported metal catalysts: Rh/Ce_{0.8}Zr_{0.2}O₂ [20], Pt/Ce_{0.8}Zr_{0.2}O₂ [21] and Pt/Ce_{0.8}Tb_{0.2}O_{2-x} [30] catalysts. In accordance with the HREM studies performed on them, metal decoration or alloying phenomena could only be observed on samples reduced at 973 K or higher temperatures. This represents a

* To whom correspondence should be addressed.

very significant difference with respect to the behaviour exhibited by the classic SMSI, titania-based, systems.

The reversibility is a major characteristic feature of the SMSI effect [8–10]. Accordingly, proving the occurrence of a true SMSI requires the regeneration of the deactivated catalyst by reoxidation followed by a milder reduction treatment. In the case of NM/TiO₂, reoxidation at about 773 K is known to be effective for recovering the catalysts from the SMSI state [8–10,31]. Probably by analogy with these earlier studies on titania-supported noble metal systems, similar reoxidation temperatures (773 K) have also been applied to NM/CeO₂ catalysts for recovering their chemisorptive and/or catalytic properties from the deactivated state [5,6,32].

In this work, with the help of HREM, digital image processing, and high-resolution analytical techniques (EELS), we report on the nanoscale changes induced on decorated/alloyed NM/CeO₂ (NM: Rh, Pt) catalysts by two reoxidation treatments at 773 and 1173 K. The former, as previously stated, is the reference oxidation temperature for regenerating titania-based catalysts from the SMSI state. The latter, as deduced from the results presented and discussed here, is a relevant one for ceria-supported noble metal catalysts.

2. Experimental

The ceria-supported rhodium and platinum catalysts investigated here were prepared by the incipient wetness impregnation technique from aqueous solutions of chloride-free metal precursors, Rh(NO₃)₃ and [Pt(NH₃)₄](OH)₂, respectively. A commercial powder CeO₂ sample from Alfa Ventron, 99.9% purity, and a specific surface area of 4 m² g⁻¹, was used as support. The metal loadings for Rh/CeO₂ and Pt/CeO₂ catalysts were, respectively, 2.5 and 4 wt%. After the impregnation step, the catalysts were dried in air at 398 K and stored in a desiccator until used.

Reduction and oxidation treatments were carried out by heating the catalysts, from room temperature up to the selected temperature in a flow of pure H₂ or O₂, respectively. The heating rate was always 10 K min⁻¹.

The onset of the deactivated (decorated or alloyed) state in the Rh/CeO₂ and Pt/CeO₂ samples was induced by reducing them for 1 h, at 1173 K, in a flow of pure H₂. Then, they were flushed with He, for 1 h, at 1173 K, finally, they were cooled to 298 K, also in a flow of inert gas.

The reoxidation treatments applied to these heavily reduced samples consisted of heating them in a flow of pure O₂ from 298 to 773 or 1173 K, then, they were kept under flowing O₂ for 1 h at the selected reoxidation temperature, and finally, they were cooled to 298 K always in a flow of O₂. After completing the reoxidation treatment the samples were re-reduced for 1 h in a flow of pure H₂ at 623 K, then, they were evacuated for 1 h under flowing He, at 773 K, and cooled to room temperature also in a flow of the inert gas.

To prevent the fast and uncontrolled reoxidation of the reduced catalysts during their transfer to the electron micro-

scope chamber, they were passivated as follows: the samples were cooled to 191 K (solid–liquid acetone trap) in a flow of He; then the gas flow was switched to O₂ (5%)/He; after 0.5 h of treatment with this oxidising mixture at 191 K, they were slowly warmed up to 298 K, and finally, they were rapidly transferred to the microscope.

For their observation in the electron microscope, the catalyst powders were dispersed on holey carbon Cu grids using the procedure described elsewhere [26].

The high-resolution electron microscopy (HREM) study was performed in a JEOL 2000EX transmission electron microscope (200 keV accelerating voltage, Cs = 0.7 mm) with a 0.21 nm structural resolution. The images were recorded, at 600 Kx magnification, on KODAK 6.5 × 9 cm SO-163 photographic plates which were developed using conventional procedures. To guarantee reaching conclusions with statistical significance, at least one hundred plates were recorded for each sample. At 600 Kx, these plates cover an area roughly 120 nm × 150 nm in such a way that some tens of particles are usually imaged in one of these plates. In these conditions the structural features which will be commented throughout the paper can be considered as representative of the state of the samples under study.

For their quantification and analysis, selected regions of these micrographs were digitised using a COHU-4910 CCD camera (768 × 512 pixels, 256 grey levels) and a light box. Image acquisition and analysis were carried out using different routines developed in our laboratory and coded in SEMPER6+ software from Synoptics. The diffractograms or digital diffraction patterns (DDPs) included in this work correspond to the log-scaled power spectrum of the Fourier transform of the bidimensional intensity distribution in the digitised images. Lattice fringe spacings have been measured from these DDPs by locating the maximum of intensity within the diffraction spots. Errors associated to these measurements are about ±0.015 nm for spots in the range 0.4–0.2 nm. Errors in the measurement of interplanar angles are about ±5°.

The nanoanalytical information was obtained in a VG-HB501 scanning transmission microscope (STEM) operating at 100 kV equipped with a field emission gun and a parallel detection electron energy loss spectrometer (Gatan PEELS 666). EELS spectra were processed with the EL/P program from Gatan. Specific routines developed at the Laboratoire de Physique des Solides at Orsay (Paris) were also used for on-line electron beam control during the acquisition of experimental spectra.

3. Results and discussion

Figures 1 and 2 show sequences of HREM images taken at the three steps of the reduction–reoxidation–reduction cycle for Rh/CeO₂ and Pt/CeO₂ catalysts, respectively. The purpose of the first reduction treatment at 1173 K is to induce the onset of decoration–alloying phenomena. The oxidation at 773 K is, as already noted, the classical reference

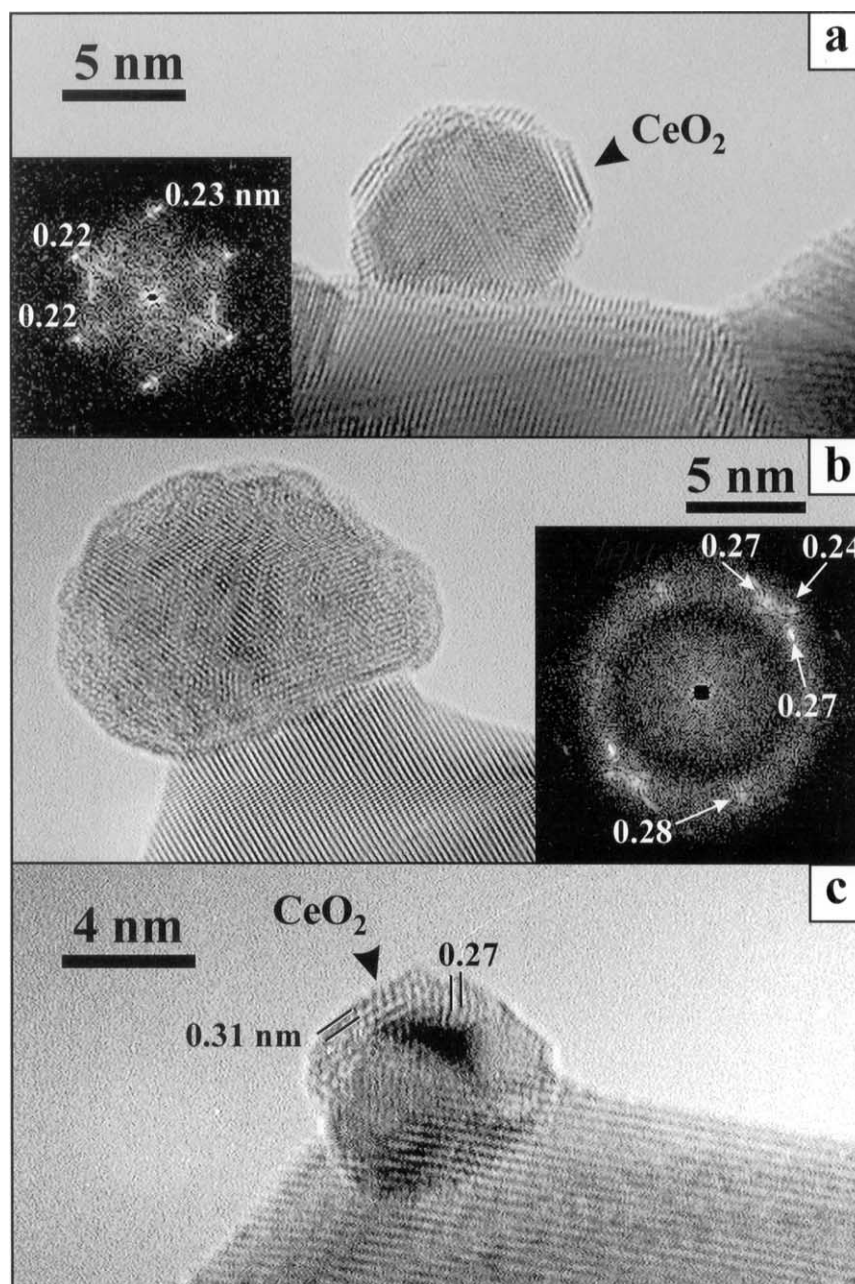


Figure 1. HREM images corresponding to the 2.5% Rh/CeO₂ catalyst after: (a) reduction at 1173 K; (b) reduction at 1173 K followed by reoxidation at 773 K; (c) reduction at 773 K, reoxidation at 773 K and further reduction at 623 K.

reoxidation treatment routinely applied in the literature for recovering the catalysts from a SMSI state. Finally the mild re-reduction, in addition to allowing the preparation of reduced metal particles, would also close the usual regeneration procedure.

As we can see in figure 1(a) for a Rh/CeO₂ catalyst, a reduction at 1173 K in pure H₂ produces metal particles whose surfaces are decorated by thin patches of the ceria support [27]. A lattice spacing of 0.312 nm, corresponding to fluorite-like ceria, can be detected in the decoration layers. The metal dispersion that can be estimated from the analysis of the particle size histogram of this sample is about 16%, much lower than that determined for the same cata-

lyst reduced at 773 K (36%) [25]. The re-oxidation treatment at 773 K of this heavily reduced Rh/CeO₂ samples, figure 1(b), leads to the formation of big, rounded shaped particles. Fringe analysis of these images using Fourier transform techniques, inset in the same figure, reveals the presence of lattice spacings in the 0.24–0.28 nm range. Such spacings cannot be due to a metallic rhodium phase but instead, as shown in table 1, they could be assigned to any of the rhodium sesquioxide phases. The complexity of the HREM contrasts, as revealed for example in the waving appearance of the fringes, and the small differences in the lattice spacing of the different oxide phases involved, preclude nevertheless an unequivocal assignment of this type of par-

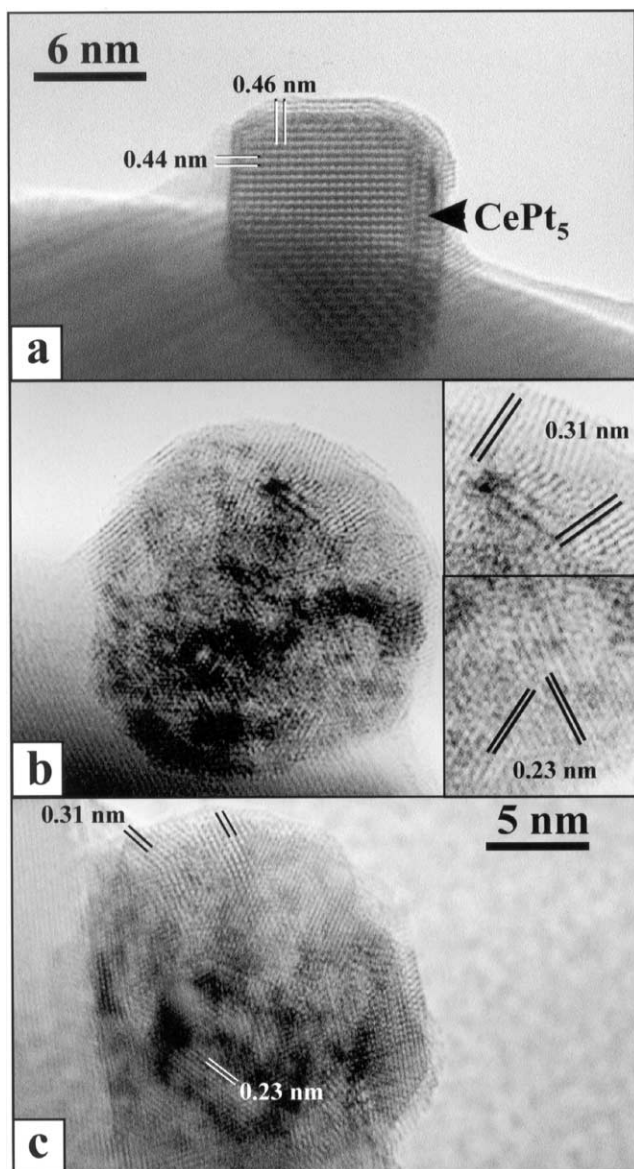


Figure 2. HREM images corresponding to the 4% Pt/CeO₂ catalyst after: (a) reduction at 1173 K; (b) reduction at 1173 K followed by reoxidation at 773 K (insets correspond to enlargements of the particle); (c) reduction at 773 K, reoxidation at 773 K and, further reduction at 623 K.

ticles to a particular oxide. Thus, the 0.27 nm value observed in the DDP could be related, within the experimental error, to any of the following family of planes: (110)-Rh₂O₃ I, (104)-Rh₂O₃ I; (002)-Rh₂O₃ II, (211)-Rh₂O₃ II; (200)-Rh₂O₃ III, (114)-Rh₂O₃ III, (020)-Rh₂O₃ III. Likewise the 0.24 nm spot could be assigned to the following possibilities: (006)-Rh₂O₃ I, (012)-Rh₂O₃ II, (021)-Rh₂O₃ II, (115)-Rh₂O₃ III, (210)-Rh₂O₃ III or (120)-Rh₂O₃ III.

Figure 3 shows an EELS spectrum which provides complementary information about the chemical composition of these particles. The spectrum was recorded in spot mode inside a particle like the one shown in figure 1(b), *i.e.*, imaged in profile. To avoid interference from the support, a region a few times the electron spot size (about 1 nm) far from the particle/support interface was analysed. As deduced from

Table 1
Some lattice spacings characteristic of rhodium, ceria and rhodium sesquioxide phases.

Phase	<i>d</i> -spacing (nm)	(<i>hkl</i>)
Rh	0.219	111
CeO ₂	0.312	111
	0.270	002
Rh ₂ O ₃ I	0.224	113
	0.231	006
	0.257	110
	0.273	104
Rh ₂ O ₃ II	0.297	210
	0.269	002
	0.260	211
	0.258	020
	0.252	102
	0.239	012
	0.233	021
Rh ₂ O ₃ III	0.299	104
	0.297	113
	0.272	020
	0.262	114
	0.257	200
	0.241	120
	0.233	210
	0.231	115

figure 3, the EELS spectrum contains the Rh-M₃ and O-K peaks, which confirms that the particle corresponds to an oxidised form of rhodium. Also important, the presence of Ce-M₄,M₅ white lines in this spectrum clearly indicates that these particles also contain cerium atoms. This result may be interpreted as due to the coexistence of ceria and oxidised rhodium in the large particles resulting from the reoxidation treatment. We conclude, accordingly, that heating in a flow of pure O₂, at 773 K, does not induce a net segregation of the support phase from the decorated metal particles.

Figure 1(c) shows the Rh/CeO₂ catalysts after the final reduction treatment. We can still see some small patches on top of the metal particles which can be identified by fringe analysis as corresponding to a fluorite-like material. In particular, in the surface patch observed on the particle depicted in figure 1(c), 0.27 nm (002)-CeO₂ and 0.31 nm (111)-CeO₂ lattice planes are identified. Hence, oxidation at 773 K, followed by a mild reduction, does not recover the catalyst from the decorated state induced on the catalyst by the reduction treatment at high temperature, 1173 K. Likewise, the metal dispersion (16%) does not change with respect to the one determined for the catalyst reduced at 1173 K.

In the case of Pt/CeO₂ catalysts, a reduction at 1173 K, figure 2(a), leads to the formation of a Pt/Ce intermetallic. As described elsewhere [23], HREM image simulation confirms the presence of nanocrystals of the CePt₅ phase with beryl-type shape. Thus, the supported particle observed in figure 1(a) shows the 0.46 and 0.44 nm lattice fringes at 90° characteristic of the [010]-CePt₅ phase. As expected, the dispersion of the supported phase after this severe treatment,

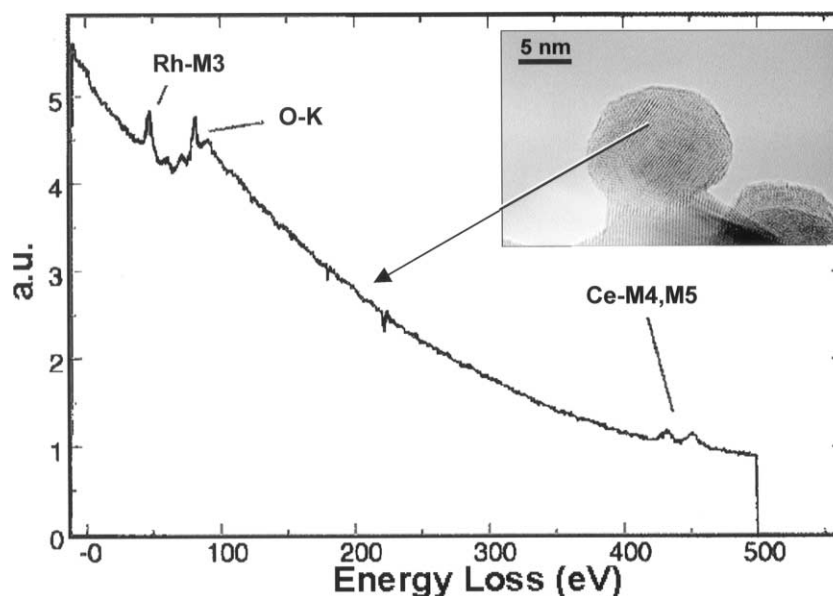


Figure 3. EELS spectrum recorded from a supported particle of the 2.5% Rh/CeO₂ catalyst reduced at 1173 K and re-oxidised at 773 K. The HREM image inset illustrates the conditions under which the signal was collected (isolated particle in profile view in a position far from the metal-support interface).

about 7.3%, is significantly lower than that observed upon reduction at 773 K, 38%. Thus, strong sintering accompanies the formation of the intermetallic CePt₅ compound.

The oxidation at 773 K with pure O₂, figure 2(b), transforms the intermetallic particles into complex aggregates. Lattice fringes running in a variety of directions are clearly visible and suggest that these particles consist of a mosaic of small, mis-oriented nanocrystals. Both (111)-Pt (0.23 nm) and (111)-CeO₂ (0.31 nm) *d*-spacings can be identified. The square insets at the right of figure 2(b) show two enlargements where these spacing can be more clearly noticed.

In the digital diffraction patterns (DDP) of these aggregates, as the one shown in figure 4, these reflections due to metallic platinum and fluorite CeO₂ are also present. The spots coming from fcc platinum are only a few whereas those related to ceria are numerous and form a ring at 0.31 nm.

These features in the HREM images and in the DDPs suggest that during the treatment in oxygen at 773 K the oxidation of the intermetallic takes place with segregation of metallic platinum and CeO₂. Moreover, the aggregates observed after this treatment seem to consist of a core of platinum, comprised of one of at least only a few fcc units, covered by a large number of nanometer-sized, randomly oriented, ceria surface patches.

A final reduction of the Pt/CeO₂ catalyst at 623 K, does not change the nanostructure of the catalyst with respect to that described in the previous paragraph and, therefore, does not prove to be effective in recovering the pure metal phase. In figure 2(c) we can observe the same complex aggregates detected after the oxidation at 773 K. They remain even with a re-reduction at higher temperature (773 K).

These observations confirm that a treatment in O₂ at 773 K is severe enough to destroy the intermetallic but does not regenerate the situation corresponding to a Pt/CeO₂ catalyst directly reduced at 773 K or lower temperatures, *i.e.*,

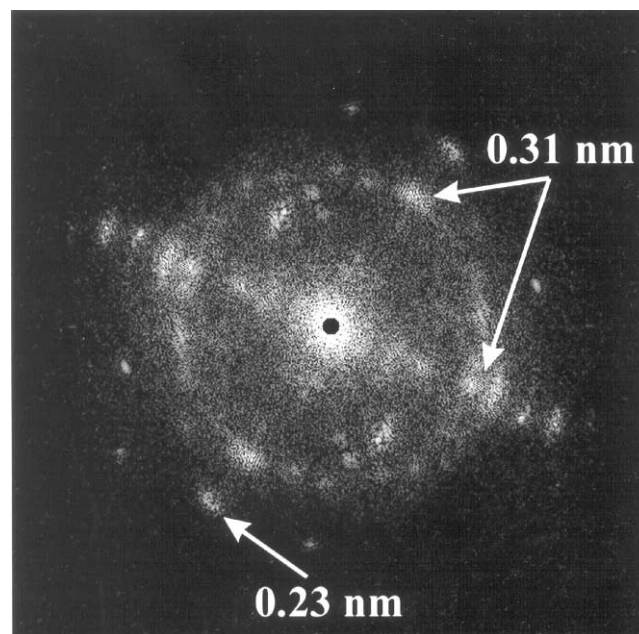


Figure 4. Digital diffraction pattern from the supported particle shown in figure 2(b).

a system consisting of small metal particles dispersed on the support. To summarise, the application of the standard regeneration treatment does not recover the Pt/CeO₂ catalyst from the alloyed state.

Figure 5 (a) and (b) shows HREM images representative of the catalysts reduced at 1173 K and further oxidised in pure O₂ at 1173 K. The structure of both catalysts is clearly different from that observed after re-oxidation at 773 K. Notice that in this case both materials seem to be formed by small, crystalline metal particles dispersed over the ceria surface. Fringe analysis confirms that these crystallites consist of metallic rhodium and platinum, respectively. Thus, the

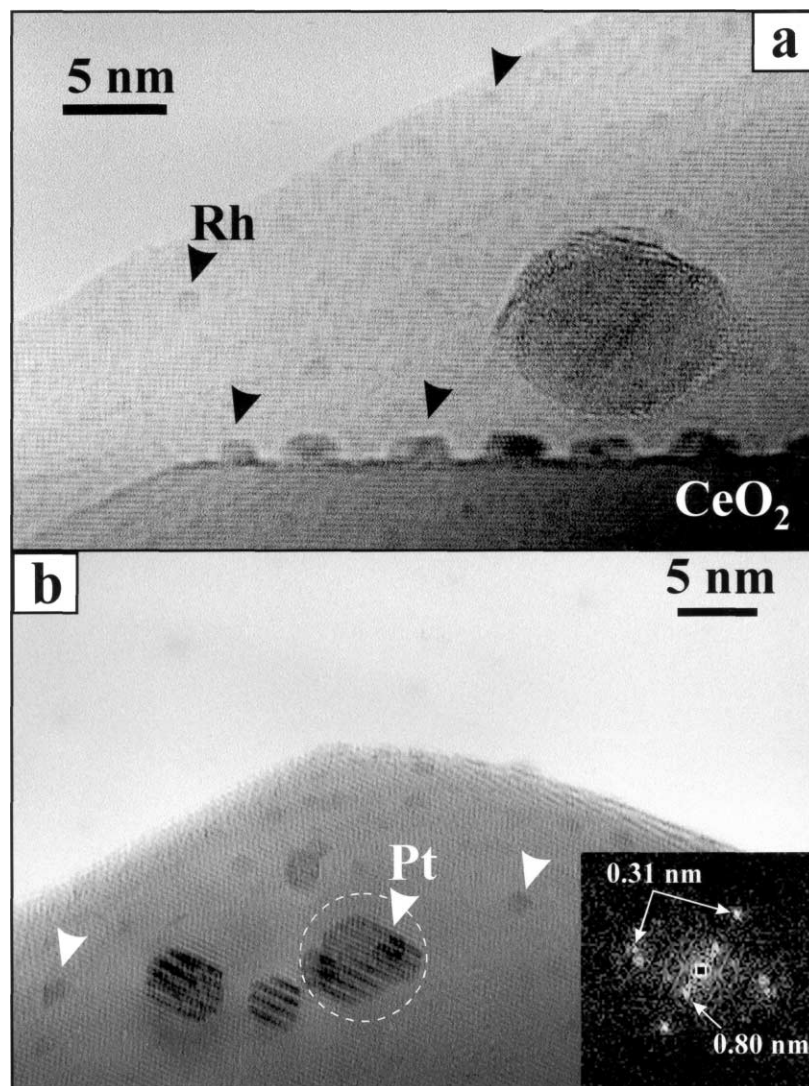


Figure 5. Representative HREM images obtained from the catalysts reduced at 1173 K and reoxidised at 1173 K: (a) 2.5% Rh/CeO₂ and (b) 4% Pt/CeO₂.

DDPs of the larger particles observed in the image of the Pt catalyst show 0.8 nm Moiré-type fringes aligned with the (111)-CeO₂ reflections. These spots arise from double diffraction in the (111)-Pt and (111)-CeO₂ planes under a parallel orientation relationship. Therefore this result, in addition to confirm the presence of metallic Pt particles in the sample oxidised at 1173 K, suggests that these particles are epitaxially grown on the support. A detailed inspection also reveals that the exposed surfaces of these particles are clean, *i.e.*, free from support overlayers.

Also worth noting is that the metal dispersion estimated from the histogram corresponding to the Rh/CeO₂ catalyst reduced at 1173 K and further reoxidised at the same temperature is 32%. This value is twice that determined for the sample directly reduced at 1173 K. Therefore, the high-temperature reoxidation treatment not only induces the recovery of the catalyst from the decorated state; it also seems to induce the rhodium redispersion.

The average diameter of the platinum particles estimated from the micrographs of the Pt/CeO₂ sample reduced at

1173 K and further oxidised at 1173 K is also smaller than that of the catalyst directly reduced at 1173 K. This observation might well be interpreted as due to platinum redispersion induced by the high-temperature reoxidation treatment. Nevertheless, additional scanning electron microscopy and EDS analytical studies carried out on the regenerated Pt/CeO₂ sample have shown the simultaneous occurrence of very large platinum particles in the micron range size. This means that, in the case of the Pt/ceria catalyst, the high-temperature reoxidation treatment, in addition to inducing the reversion from the alloyed state, leads to a severe metal sintering.

4. Conclusions

The results reported in this work clearly show that the classic reoxidation treatment at 773 K does not allow the recovery of the NM/CeO₂ catalysts from the decorated or alloyed states. The noble metal/ceria phase separation may only be achieved upon reoxidation at temperatures well

above 773 K. This observation represents an additional major difference between titania- and ceria-supported noble metal catalysts. Moreover, the likely regeneration of NM/CeO₂ catalysts reduced at 773 K by reoxidation at 773 K would actually prove, in good agreement with earlier HREM studies on the reduced catalysts [25,27], that the observed deactivation effects are not due to decoration or alloying phenomena, rather consisting of purely electronic effects [33].

Finally, the reoxidation treatment at high temperature, 1173 K, appears to be suitable for recovering the metal particles from the decorated or alloyed states. The analysis of the evolution undergone by metal particle size distributions suggests some differences in the behaviour of rhodium and platinum catalysts. Thus, the microanalytical studies performed on the platinum catalyst indicate the coexistence of a fraction of highly dispersed metal crystallites with another one consisting of very large particles, over 100 nm. In the case of the rhodium catalyst no similar evidence could be obtained, thus suggesting an effective metal redispersion.

Acknowledgement

This work has been supported by the CICYT (Project: MAT99-0570) and the Junta de Andalucía (FQM110). One of us (JAPO) acknowledges the grant received from the TMR Programme of the EU allowing him to make a long duration stay at the Laboratoire de Physique des Solides at the Paris-Sud University. The high-resolution electron microscopy images were obtained at the Electron Microscopy Facilities of the Servicios Centrales de Ciencia y Tecnología de la Universidad de Cádiz.

References

- [1] P. Meriaudeau, J.F. Dutel, M. Dufaux and C. Naccache, *Stud. Surf. Sci. Catal.* 11 (1982) 95.
- [2] P. Meriaudeau, J.F. Dutel, M. Dufaux and C. Naccache, in: *Strong Metal Support Interactions*, ACS Symp. Ser. 298 (1986) 118.
- [3] C. Leitenburg, A. Trovarelli and J. Kaspar, *Catal.* 166 (1997) 98.
- [4] C. Binet, A. Jadi, J.C. Lavalley and M. Boutonet-Kizling, *J. Chem. Soc. Faraday Trans.* 88 (1992) 2079.
- [5] D. Kalakkad, A.K. Datye and H. Robota, *Appl. Catal. B* 1 (1992) 191.
- [6] A. Trovarelli, G. Dolcetti, C. Leitenburg, J. Kaspar, P. Finetti and A. Santoni, *J. Chem. Soc. Faraday Trans.* 88 (1992) 1311.
- [7] J. Cunningham, S. O'Brien, J. Sanz, J.M. Rojo, J. Soria and J.L.G. Fierro, *J. Mol. Catal.* 57 (1990) 379.
- [8] S.J. Tauster, S.C. Fung and R.L. Garten, *J. Am. Chem. Soc.* 100 (1978) 170.
- [9] S.J. Tauster, *Acc. Chem. Res.* 20 (1987) 389.
- [10] G.L. Haller and D.E. Resasco, *Adv. Catal.* 36 (1989) 173.
- [11] A. Bensalem, J.C. Muller, D. Tessier and F. Bozon-Verduraz, *J. Chem. Soc. Faraday Trans.* 92 (1996) 3233.
- [12] J. Cunningham, D.S. Cullinane, J. Sanz, J.M. Rojo, J. Soria and J.L.G. Fierro, *J. Chem. Soc. Faraday Trans.* 88 (1992) 3233.
- [13] J. Barrault, A. Alouche, V. Paul-Boncour, L. Hilaire and A. Percheron-Guegan, *Appl. Catal.* 46 (1989) 269.
- [14] P.J. Levy and M. Primet, *Appl. Catal.* 70 (1991) 263.
- [15] S. Bernal, M.A. Cauqui, G.A. Cifredo, J.M. Gatica, C. Larese and J.A. Pérez-Omil, *Catal. Today* 29 (1996) 77.
- [16] S. Bernal, J.J. Calvino, M.A. Cauqui, G.A. Cifredo, A. Jobacho and J.M. Rodríguez-Izquierdo, *Appl. Catal.* 99 (1993) 1.
- [17] D.I. Kondarides and X.E. Verykios, *J. Catal.* 174 (1998) 52.
- [18] A. Pfau, J. Sanz, K.D. Schiervau, W. Göpel, J.P. Belzunegui and J.M. Rojo, *Stud. Surf. Sci. Catal.* 101 (1996) 931.
- [19] P. Fornasiero, J. Kaspar and M. Graziani, *J. Catal.* 167 (1997) 576.
- [20] J.M. Gatica, R.T. Baker, P. Fornasiero, S. Bernal, G. Blanco and J. Kaspar, *J. Phys. Chem. B* 104 (2000) 4667.
- [21] J.M. Gatica, R.T. Baker, P. Fornasiero, S. Bernal and J. Kaspar, *J. Phys. Chem. B* 105 (2001) 1191.
- [22] A.K. Datye, D. Kalakkad, M.H. Yao and D.J. Smith, *J. Catal.* 155 (1995) 148.
- [23] S. Bernal, J.J. Calvino, J.M. Gatica, C. Larese, C. López-Cartes and J.A. Pérez-Omil, *J. Catal.* 169 (1997) 510.
- [24] D. Kalakkad, A.K. Datye and H.J. Robota, *J. Catal.* 148 (1994) 729.
- [25] S. Bernal, J.J. Calvino, M.A. Cauqui, J.M. Gatica, C. Larese, J.A. Pérez-Omil and J.M. Pintado, *Catal. Today* 50 (1999) 175.
- [26] S. Bernal, J.J. Calvino, J.A. Cauqui, Pérez-Omil, J.M. Pintado and J.M. Rodríguez-Izquierdo, *Appl. Catal. B* 16 (1998) 127.
- [27] S. Bernal, F.J. Botana, J.J. Calvino, G.A. Cifredo, J.A. Pérez-Omil and J.M. Pintado, *Catal. Today* 23 (1995) 219.
- [28] S. Bernal, F.J. Botana, J.J. Calvino, M.A. Cauqui, G.A. Cifredo, A. Jobacho, J.M. Pintado and J.M. Rodríguez-Izquierdo, *J. Phys. Chem.* 97 (1993) 4118.
- [29] S. Bernal, G. Blanco, J.J. Calvino, G.A. Cifredo, J.A. Pérez-Omil and J.M. Pintado, *Stud. Surf. Sci. Catal.* 82 (1994) 507.
- [30] G. Blanco, J.J. Calvino, M.A. Cauqui, P. Corchado and C. López-Cartes, *Chem. Mater.* 11 (1999) 3610.
- [31] S. Bernal, F.J. Botana, J.J. Calvino, C. López-Cartes, J.A. Pérez-Omil and J.M. Rodríguez-Izquierdo, *J. Chem. Soc. Faraday Trans.* 92 (1996) 2799.
- [32] D.W. Daniel, *J. Phys. Chem.* 92 (1988) 3891.
- [33] S. Bernal, G. Blanco, J.M. Gatica, C. Larese and H. Vidal, *J. Catal.* 200 (2001) 411.